

Amyloid Histology Stain for Rapid Bacterial Endospore Imaging^{∇†}

Bing Xia,¹ Srigokul Upadhyayula,^{2,3} Vicente Nuñez,² Pavel Landsman,¹ Samuel Lam,³
Harbani Malik,² Sharad Gupta,² Mohammad Sarshar,² Jingqiu Hu,¹
Bahman Anvari,² Guilford Jones,¹ and Valentine I. Vullev^{2,3,4*}

Department of Chemistry and Photonics Center, Boston University, Boston, Massachusetts 02215¹; Department of Bioengineering and Center for Bioengineering Research, University of California, Riverside, California 92521²; Department of Biochemistry, University of California, Riverside, California 92521³; and Department of Chemistry, University of California, Riverside, California 92521⁴

Received 11 November 2010/Returned for modification 24 January 2011/Accepted 19 May 2011

Bacterial endospores are some of the most resilient forms of life known to us, with their persistent survival capability resulting from a complex and effective structural organization. The outer membrane of endospores is surrounded by the densely packed endospore coat and exosporium, containing amyloid or amyloid-like proteins. In fact, it is the impenetrable composition of the endospore coat and the exosporium that makes staining methodologies for endospore detection complex and challenging. Therefore, a plausible strategy for facile and expedient staining would be to target components of the protective surface layers of the endospores. Instead of targeting endogenous markers encapsulated in the spores, here we demonstrated staining of these dormant life entities that targets the amyloid domains, i.e., the very surface components that make the coats of these species impenetrable. Using an amyloid staining dye, thioflavin T (ThT), we examined this strategy. A short incubation of bacillus endospore suspensions with ThT, under ambient conditions, resulted in (i) an enhancement of the fluorescence of ThT and (ii) the accumulation of ThT in the endospores, affording fluorescence images with excellent contrast ratios. Fluorescence images revealed that ThT tends to accumulate in the surface regions of the endospores. The observed fluorescence enhancement and dye accumulation, coupled with the sensitivity of emission techniques, provide an effective and rapid means of staining endospores without the inconvenience of pre- or posttreatment of samples.

This article describes the use of a benzothiazole dye, thioflavin T (ThT) (Fig. 1), for expedient and facile fluorescence staining of bacillus endospores. Using fluorescence microscopy and spectroscopy, we examined the capabilities of ThT to stain the endospores of four bacterial species. Our findings showed that the observed efficient staining resulted from (i) an increase in the emission quantum yield of ThT upon its uptake by endospores and (ii) a high propensity of ThT to accumulate in the endospores.

Bacterial endospores are some of the most resilient living entities known (8, 14, 57). Although the majority of the sporulating species are not virulent, spore-forming bacteria produce the most potent toxins known to humans, such as botulinum toxin (2, 55). This potential threat of highly virulent biohazards, along with their resistance to treatment, places a demand for rapid and simple bioanalytical methods for detection of bacterial endospores. Such robust bioanalytical methods are not only essential for biodefense but also relevant to clinical and microbiological applications (1, 29, 66, 70).

The classical technique of endospore detection uses malachite green dye to stain the endospore coat via thermal treatment or long incubation periods (71). Genetic bioassays utilizing PCR have since evolved to provide the specificity required

for identification of certain sporulating pathogens (5, 19, 52, 68). Employing these techniques for detection of bacterial endospores, however, is a multistep process and requires prior sequence knowledge for the design of the primer (30, 44, 87).

Other signal amplification techniques, such as enzyme-linked immunosorbent assay (ELISA), provide sensitivity for detection of endospore pathogens with potentially high specificity, without tedious sample pretreatment (77, 80). Endospore immunoassays, however, require (i) identification of a protein or another biomarker at the surface of the endospore particles and (ii) development of immunoglobulins (i.e., antibodies) for that surface biomarker (30, 65, 87). In order to reliably identify endospores, the immunoassays often require a severalfold higher concentration than the infectious dose or several distinct antibodies to detect one of several strains of the same sporulating pathogenic species (18, 48, 65, 95).

A variety of optical and mass spectrometry techniques have been explored for detection of bacterial endospores without requiring signal amplification biochemical reactions. For example, surface-enhanced Raman spectroscopy (SERS) brings the level of detection to a relatively low spore count and even to a single spore (64, 99). Mass spectrometry provides a means for identification of macromolecular markers based on their exact masses (6, 78). The specialized equipment that is needed, along with the complexity of the data analysis, has proven prohibitive for the wide deployment of such bioanalytical methodologies into the clinical field.

For the last decade, dipicolinic acid (DPA) has gained considerable popularity as a marker for the detection of bacterial endospores (16, 22, 25, 59, 67, 83, 92, 97). Emission enhance-

* Corresponding author. Mailing address: Department of Bioengineering, University of California, Riverside, 900 University Avenue, Riverside, CA 92521. Phone: (951) 827-6239. Fax: (951) 827-6416. E-mail: vullev@ucr.edu.

† Supplemental material for this article may be found at <http://jcm.asm.org/>.

[∇] Published ahead of print on 8 June 2011.

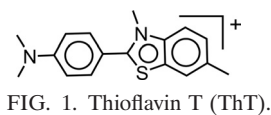


FIG. 1. Thioflavin T (ThT).

ment assays for DPA and bacterial endospores, utilizing lanthanide ions, were developed at the U.S. Army Research Laboratory at the end of the 20th century (59, 67) and were recently improved by a research team at the Jet Propulsion Laboratory (9, 10). Up to about 20% of the weight of bacterial endospores can be attributed to calcium dipicolinate: i.e., DPA is a natural product observed solely in sporulated bacterial species (75, 76). Furthermore, DPA has a high affinity for chelating lanthanide metal ions, such as terbium(III) (36, 37). Excitation of the DPA ligands at about 270 nm to 280 nm, wavelengths at which the lanthanides do not exhibit allowed spectral transitions, permits selective photoexcitation of the DPA-chelated ions. This selective photoexcitation of DPA, followed by a fast energy transfer from the DPA ligands to the chelated ions, results in luminescence predominantly from the lanthanides that are in a complex with DPA.

These lanthanide emission assays are general for all bacterial endospores and do not provide discernment between virulent and benign sporulated species. However, the simplicity, cost efficiency, and relative sensitivity make these emission enhancement techniques a preferred choice for the first line of defense, that is, for monitoring the environmental endospore content. Abnormal fluctuations, such as an increase in the spore count in the environment, would call for deployment of more costly bioanalytical technologies with higher specificity. Due to their expedience and relative simplicity, lanthanide emission enhancement approaches are also deployed for assaying alternative biomarkers with clinical importance (16).

The use of DPA as an endogenous biomarker requires sample pretreatment to lyse the endospores for extracting their content without chemically deteriorating it. The resilience of bacterial endospores, however, makes the DPA extraction step, which requires heat treatment, surfactant additives, or microwaving, a source of potential irreproducibility in the quantification of the results. Furthermore, the lysing of the endospores, as a pretreatment for extraction of the DPA, makes this bioanalytical approach unfeasible for imaging applications.

Alternative biomarkers, which are in abundance on the surface of the endospore particulates, will provide venues for facile detection without the requirement for lysing pretreatment of the samples. High-resolution scanning probe images, for example, revealed significant abundance of β -sheet amyloid-like proteins on the surfaces of bacterial endospores (60–63). Amyloid folds are, indeed, intricate components of bacterial cell walls and endospore coatings (17, 20, 23, 42, 60–63).

Amyloid fibrils are aggregated filamentous protein structures found in more than 20 diseases, including amyloidosis and several neurodegenerative disorders, such as Alzheimer's disease and Parkinson's disease (13, 23, 31, 51, 96). The structural properties of amyloid fibrils and the kinetics of their formation have been objects of intensive investigation. Among the techniques developed in the field, amyloid fluorescence stains have served as the dominant method. Among the amy-

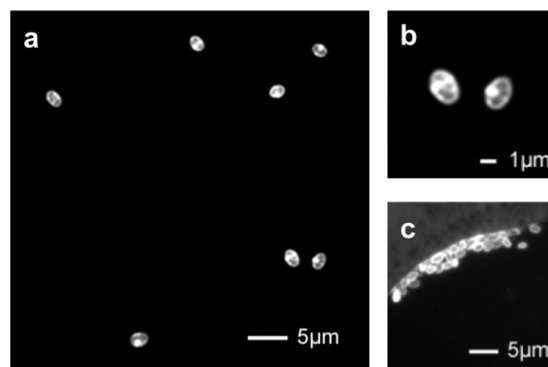


FIG. 2. Epifluorescence microscopy images of bacterial endospores of *B. atrophaeus* (a, b) and *G. stearothermophilus* (c). All endospore samples were imaged while suspended in 150 μ M ThT aqueous solution (2 mM Tris buffer, pH 8.5; exposure time = 5 s). The spores were incubated in the ThT solution for 10 min prior to imaging.

loid stains, thioflavin T (ThT) is the most widely used (7). Furthermore, ThT does not interact with folded or partially folded monomeric proteins, soluble oligomers, or amorphous aggregates (49). Changes in ThT fluorescence are imperceptible even if interactions with such impurities in the sample occur (43, 45, 49, 53, 56, 58, 89).

Due to the relatively high inherent sensitivity of emission techniques, fluorescence staining and imaging are the foundation for widely preferred bioanalytical methodologies (47, 50). Herein, we explored the possibility for fluorescence staining of bacterial endospores with ThT (Fig. 1). In this study, we focused on *Bacillus subtilis* and *Bacillus globigii*, which are phylogenetically related organisms that are frequently explored as models for virulent bacilli. In addition, we used *Bacillus atrophaeus* and *Geobacillus stearothermophilus*, which form relatively large endospores that are suitable for optical imaging.

For the staining, we relied on the specificity of ThT for amyloid folds as endogenous markers occurring on bacterial endospore surfaces and in the cell walls of vegetative bacteria. The lack of requirements for sample pretreatment not only provided expedience but also allowed for preserving the bacterial entities intact, which is essential for imaging. We observed a high contrast between the ThT-stained bacterial endospores and the free dye remaining in the surrounding solution (Fig. 2). Therefore, a sample wash was not required after the staining and prior to imaging, which was another important factor contributing to the expedience of this approach. Our analysis revealed that the reasons for the observed high contrast of the fluorescence images of the bacterial species are (i) an increase in emission quantum yield of ThT upon binding to bacterial endospores and (ii) a high affinity of ThT for components of the examined bacterial species, leading to accumulation of the dye in the imaged bacteria: i.e., the concentration of ThT in the stained endospores was more than three orders of magnitude larger than the concentration of ThT in the surrounding staining solution.

MATERIALS AND METHODS

Materials. The reagents and solvents (spectroscopic grade) were purchased from VWR, Fisher Scientific, and Sigma-Aldrich. Bacteria for endospore cultures were obtained as follows: (i) *B. subtilis*, *B. globigii*, and *Bacillus thuringiensis*

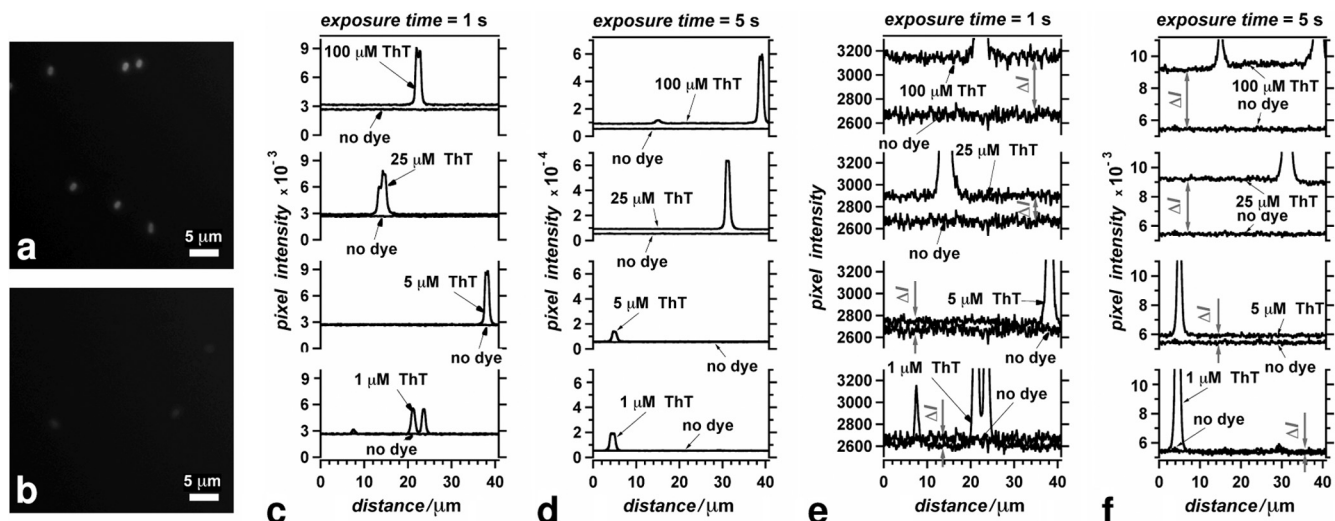


FIG. 3. Gray-scale analysis (84) of epifluorescence microscopy images of *B. atrophaeus* endospores suspended in solutions with various concentrations of ThT (2 mM Tris buffer, pH 8.5). (a, b) Fluorescence images (exposure time = 5 s) in the presence of 1 μM ThT (a) and with no dye present (b). (c, d) Traces from images of spores suspended in different concentrations of ThT recorded at exposure times of 1 s (c) and 5 s (d). (e, f) The same traces as shown in panels c and d plotted against expanded ordinates, demonstrating the differences between the baselines of the images with and without dye, ΔI . ΔI represents the contribution of the fluorescence from the free ThT to the backgrounds of the microscope images, A_{DC} . (ΔI values were 490, 240, 60, and <20 for 100 μM , 25 μM , 5 μM , and 1 μM ThT at an exposure time of 1 s, and ΔI values were 4,100, 3,300, 460, and <50 for 100 μM , 25 μM , 5 μM , and 1 μM ThT at an exposure time of 5 s.) The peak signals corresponding to the spores labeled with ThT (i.e., to the dye taken up by the spores) exceed the background fluorescence, ΔI , by more than an order of magnitude, $(\Delta h) + \Delta I/\Delta I > 10$. For 1-s exposure time, the baseline RMS values were 35, 24, 32, 25, and 35 for 0 μM , 1 μM , 5 μM , 25 μM , and 100 μM ThT, and for 5-s exposure time, the root mean square (RMS) values were 75, 65, 92, 96, and 120 for 0 μM , 1 μM , 5 μM , 25 μM , and 100 μM ThT.

were obtained as desiccated powders from the U.S. Army Research Laboratory facility, and (ii) *B. atrophaeus* and *G. stearothermophilus* were purchased from SPS Medical (Rush, NY) in the form of 20% ethanol aqueous suspensions. Vegetative bacterial cultures of *Escherichia coli* TOP10 cells were obtained from Invitrogen (Carlsbad, CA), and wild-type *B. subtilis* was obtained from the ATCC (Manassas, VA). For details on sample preparation and handling, see the supplemental material.

Optical imaging. Bright-field and fluorescence images were acquired using a Nikon Ti-U inverted microscope (Nikon, Inc., Melville, NY), equipped with a 100 \times Nikon oil immersion objective (numerical aperture, 1.49; working distance [WD], 120 μm) and a Hamamatsu electron multiplier charge-coupled-device digital camera (model C9100-13; Hamamatsu Corp., Bridgewater, NJ). Image analysis of the gray-scale distribution was performed using Igor Pro software version 6.02A (WaveMetrics) installed on Windows and Mac OS workstations as we have previously demonstrated (11, 27, 54, 84, 85). (For details, see the supplemental material.)

Spectroscopy. Absorption spectra were recorded using a Jasco V-670 UV-visible-noninfrared (UV/Vis/NIR) spectrophotometer and a DU-640B Beckman spectrophotometer. Steady-state emission spectra were recorded using a Fluorolog-3-22 spectrofluorometer (Horiba Jobin Yvon), with slit widths between 2 and 5 nm, and a Felix/TimeMaster spectrofluorometer (Photon Technology International, Inc.), with a 10-nm slit width (32–35, 38, 40, 91). The thioflavin T concentrations for all samples were estimated from the apparent molar absorption coefficient of ThT at a peak wavelength of 412 nm ($36,000 \pm 500 \text{ M}^{-1} \text{ cm}^{-1}$) (21). (Further experimental details are available in the supplemental material.)

RESULTS

Staining of bacterial endospores with ThT. Treatment of bacterial samples with ThT allows for visualization of the endospores via fluorescence microscopy, employing an excitation wavelength shorter than about 450 nm (Fig. 2). For the staining, which tends to be completed in less than 5 min as we previously reported (86), we incubated the bacterial samples in dye solutions at micromolar concentrations. The background fluorescence from the ThT (free in solution) was significantly

less intense than the fluorescence from the stained endospores (Fig. 3). Therefore, no washing of the staining dye, which was left over in the sample solution, was required in order to attain good-quality images.

In fluorescence microscope images, the noise has direct current (DC) and alternating current (AC) components. The AC and DC contributions to the signal-to-noise (S/N) ratio were estimated separately using the noise amplitudes and the average heights, $\langle h \rangle$, of the peaks on the traces crossing over imaged spores (Fig. 3):

$$S/N_{DC} \text{ (dB)} = 20 \lg \left(\frac{\langle h \rangle}{A_{DC}} \right) \quad (1)$$

$$S/N_{AC} \text{ (dB)} = 20 \lg \left(\frac{\langle \Delta h \rangle}{\text{RMS}} \right) \quad (2)$$

where the multiple of 10 in front of the logarithms converts the units to decibels, and $\langle \Delta h \rangle = \langle h \rangle - A_{DC}$.

Signal-to-noise ratio analysis revealed key trends in the quality of the images recorded under different settings and staining conditions. As expected, the S/N ratio increased with the prolongation of the exposure time, $S/N \propto \sqrt{\text{exposure time}}$. A 5-fold increase in the exposure time doubled the S/N_{DC} and caused about a 30% increase in the S/N_{AC} of images of spores suspended in 100 μM ThT (see the supplemental material).

Imaging of relatively large bacterial endospores (i.e., endospores larger than about 1 μm) revealed their contours and provided information about their shapes and dimensions (Fig. 2). For organisms that form endospores with submicrometer dimensions, the size of the imaged endospores approached the diffraction limit of optical microscopy, and their shapes and

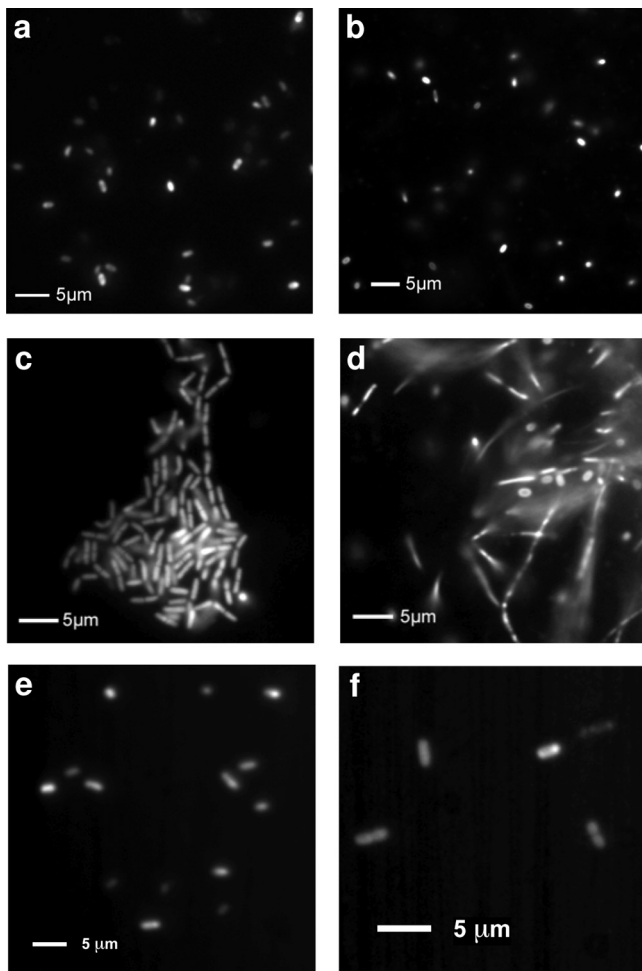


FIG. 4. Epifluorescence microscopy images of *B. globigii* endospores (a), *B. subtilis* endospores (b), *B. subtilis* vegetative cells (c), *B. subtilis* during sporulation (d), and *E. coli* cells (e, f). All bacterial samples were imaged while suspended in 150 μM ThT aqueous solution (2 mM Tris buffer, pH 8.5). The bacteria were incubated in the ThT solution for 10 min prior to imaging.

dimensions could not be always extracted with sufficient precision (Fig. 4).

Examination of the fluorescence images of the stained bacterial endospores, which were large enough for visualizing their shapes via optical microscopy, revealed (i) consistently bright pixels following the contours of the endospores and (ii) bright spots distributed throughout the endospore images (Fig. 2). The latter observation suggested a heterogeneous distribution of the endogenous biomarkers (e.g., β-sheet proteins) that are targeted by the amyloid stain. The former finding suggested that the coating layers of the endospores had a pronounced propensity for accumulating the staining dye. Our observation for surface accumulation of ThT was consistent with the abundance of β-sheet proteins found on the endospore surfaces (23, 60–63).

Amyloid-type proteins, however, are native not only to the endospore surfaces but also to the cell walls of vegetative bacteria (including the Gram-positive, spore-forming species) (17, 20, 23, 42). While ThT provided an excellent basis for

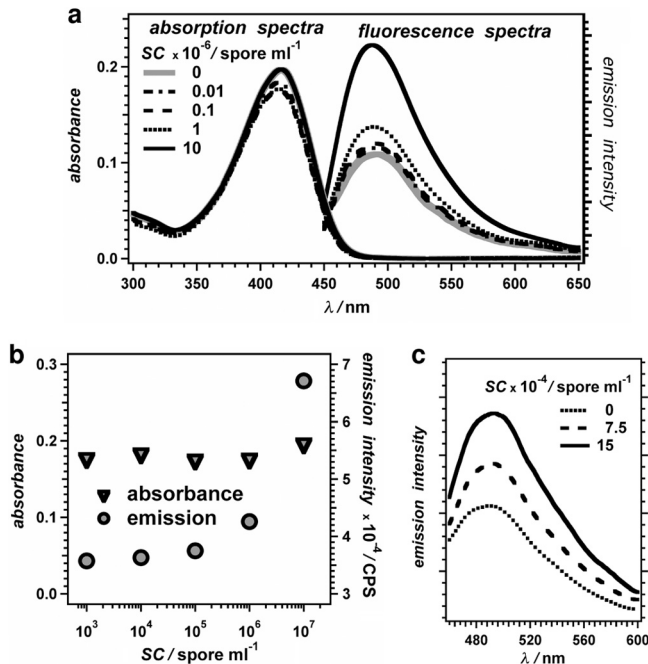


FIG. 5. Absorption and fluorescence properties of ThT (11 μM) dissolved in aqueous solutions (2 mM Tris buffer, pH 8.5; absorption and excitation optical path length = 0.5 cm) in the absence and presence of different amounts of bacterial endospores (SC = spore count): (a) absorption and emission (λ_{ex} = 430 nm) spectra of ThT samples containing *B. atrophaeus* with different SCs (for SC exceeding 10⁷ spores ml⁻¹, the baseline of the absorption spectra in the blue and UV region shifts due to scattering); (b) dependence of the absorbance (λ_{abs} = 415 nm) and emission intensity (λ_{ex} = 415 nm, λ_{em} = 490 nm) on the spore count; (c) emission spectra of ThT in the presence and absence of *B. globigii* endospores (λ_{ex} = 430 nm).

staining bacterial endospores with considerable ease (at ambient temperature and with no sample pretreatment or posttreatment), it also stained vegetative bacteria, both Gram positive (Fig. 4c) and Gram negative (Fig. 4e and f). The morphologies of vegetative bacterial cells and their endospores, however, are quite different, and they can be readily discerned from each other by comparing their shapes and sizes even when they are in the same sample (Fig. 4d, sporulating bacteria).

Spore-induced emission enhancement of ThT. The brightness of a fluorescence image depends on the number of dye molecules at the focal plane (or in the vicinity of the focal plane) and on the emission quantum yield of the dye. The number of molecules within the focal volume of illumination (i.e., the local concentration of the dye) determines how much of the excitation light is absorbed. Concurrently, the emission quantum yield determines how much of the absorbed light is emitted by the dye (at wavelengths longer than the excitation wavelength, λ_{ex}). Therefore, potential reasons for the observed fluorescence staining of the bacterial endospores with ThT include an increase in the emission quantum yield of ThT upon binding to the endospores and accumulation of ThT in the endospores.

Upon addition of endospores to the ThT solution, we observed an increase in its emission intensity without significant change in its optical density at the excitation wavelength (Fig. 5). This finding indicated that an increase in the ThT emission

quantum yield was one of the factors governing the observed emission enhancement upon endospore uptake of the dye.

The observed emission enhancement phenomenon, induced by the endospore uptake, is consistent with the sensitivity of the photophysical properties of ThT to the viscosity of the environment: i.e., the emission quantum yield of ThT increases with the increase in the medium viscosity (72, 74, 81, 82, 88, 90). Due to the single carbon-carbon bond between the two ring systems and the single carbon-nitrogen bond between the phenyl ring and the dimethyl amine (Fig. 1), ThT is a molecular rotor (24, 73, 74, 81). Similar to other chromophores that are molecular rotors (3, 4, 28, 39) within the lifetime of the lowest singlet-excited state of the dye, a viscous microenvironment slows and/or completely restrains the attainment of ThT conformers (i.e., rotamers) that have the density of vibrational states allowing efficient internal conversion to the ground state. Such viscosity-induced suppression of efficient nonradiative deactivation results in an increase in the emission quantum yield of ThT, as demonstrated by photophysical studies of this staining agent for solvent media with differing viscosities (82). Binding of ThT to protein aggregates (or other macromolecular assemblies) has a restrictive effect on its modes of molecular motion that is similar to the effect of increased medium viscosity: i.e., the binding sites provide a microenvironment with relatively high effective viscosity and cause an increase in the fluorescence quantum yield of ThT (82).

For micromolar dye concentrations, the extent of emission enhancement steadily increased with the increase in the spore count (SC) in the suspension (Fig. 6). This SC dependence of the emission intensity was consistent with an increase in the concentration of the spore-bound ThT, which has a larger fluorescence quantum yield than the free ThT in the aqueous media. The power law representing the relation between fluorescence intensity and fluorophore concentration (94) provided an excellent fit for the dependence of the observed emission enhancement on the spore count (Fig. 6c):

$$F(SC) = \Delta F(1 - 10^{-\alpha SC}) + F_0 \quad (3)$$

where $F(SC)$ is the emission intensity of ThT for the spore count, F_0 is the emission intensity of ThT in the absence of endospores, and ΔF and α depend on the photophysical properties of the dye. As depicted by the Bouguer-Lambert-Beer law (also known as Beer's law), while absorbance at the excitation wavelength, $A(\lambda_{ex})$, is linearly proportional to the fluorophore concentration, $A(\lambda_{ex})$ is logarithmically related to the intensity of the absorbed light. Therefore, broadly used linear correlations between fluorescence intensity and fluorophore concentration are an approximation of a power law: i.e., $F(SC) \propto \alpha SC$ is an approximation of equation 3. The fluorescence intensity, $F(SC)$, depends on the concentration of ThT taken up by the endospores. Hence, for the spore count range, in which $F(SC)$ versus SC follows the power law (equation 3), SC had to be linearly proportional to the concentration of ThT bound to the endospores.

Statistical tests for the presence of autocorrelation features, not depicted by the data fits, provide the means for examining the appropriateness of the fitting models for the examined data sets. An ideal model for data analysis results in random distribution of the data points around the regressed values for the

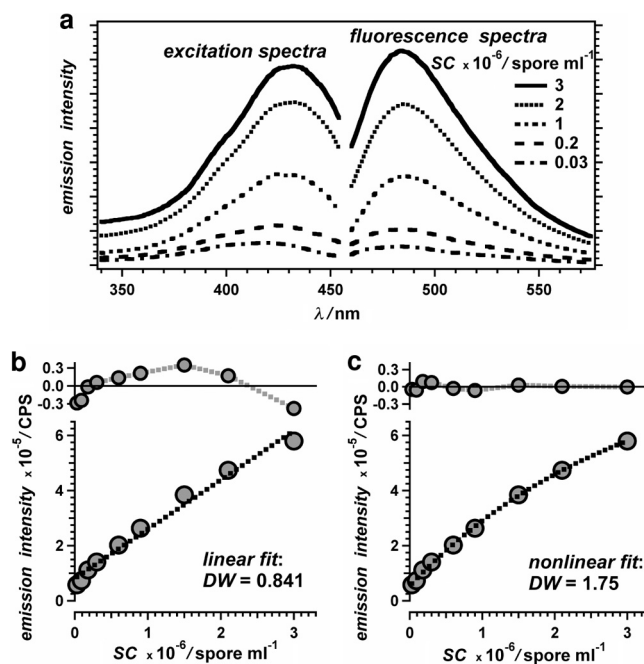


FIG. 6. Fluorescence properties of ThT (1 μ M) dissolved in aqueous solution (4 mM glycine buffer, pH 9.0) in the presence of different amounts of *B. subtilis* endospores: (a) excitation ($\lambda_{em} = 480$ nm) and emission ($\lambda_{ex} = 430$ nm) spectra; (b, c) dependence of the emission intensity ($\lambda_{ex} = 430$ nm) on the spore count (SC). The circles represent the emission intensity at 480 nm, and the dotted lines are data fits. The residuals from the data fits are plotted against a separate ordinate above the data. (b) Linear analysis of the fluorescence dependence on the spore count: $F(SC) = F_0 + \Delta F SC$. (c) Nonlinear analysis employing a power law function (equation 3) to fit the fluorescence dependence on SC. The appropriateness of the function used for data fits was examined using the Durbin-Watson test statistics:

$$DW = \frac{\sum_{i=2}^n (\delta_i - \delta_{i-1})^2}{\sum_{i=1}^n \delta_i^2}, \text{ where } \delta_i \text{ are the residual values at data points } i, \text{ and } n \text{ is the total number of data points.}$$

data fit function: i.e., the data fit residuals should not exhibit autocorrelation. Durbin-Watson statistics, DW, provide the means for examining the presence of autocorrelation. DW can assume values between 0 and 4; a DW close to 2 signifies no autocorrelation, and a DW close to 0 indicates a positive autocorrelation (15, 26, 69, 93). In particular, a DW lower than a critical value with statistical significance α , $dwL_{\alpha,k}$, indicates a positive autocorrelation in the residuals from data fits with k regression parameters, in addition to the intercept. Concurrently, a DW of $>dwU_{\alpha,k}$ indicates no autocorrelation. For linear fits, $k = 1$, and for the nonlinear power function fits (equation 3), $k = 2$. (The critical values $dwL_{\alpha,k}$ and $dwU_{\alpha,k}$ are obtained from Durbin-Watson significance tables for α , k , and for the number of examined data points n .) For the data set presented in Fig. 6b and c, $\alpha = 0.01$ and $n = 9$, $dwL_{0.01,1} = 0.554$ and $dwU_{0.01,1} = 0.998$ (for linear fits), and $dwL_{0.01,2} = 0.408$ and $dwU_{0.01,2} = 1.39$. For linear analysis, $DW = 0.841$ (Fig. 6b) and $dwL_{0.01,1} < DW < dwU_{0.01,1}$ indicated inconclusiveness in rejecting the presence of autocorrelation. Employing nonlinear analysis yielded $DW = 1.75$ (Fig. 6c) and $DW > dwU_{0.01,2}$, proving a lack of autocorrelation with at least 99%

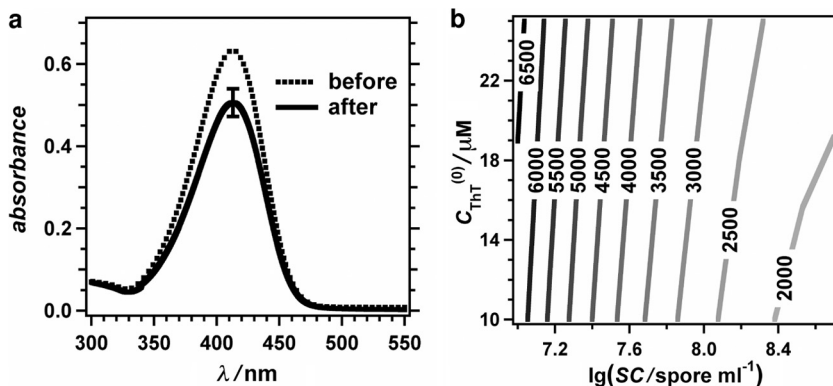


FIG. 7. Distribution coefficient, K_D (equation 4), of ThT for endospores of *B. globigii* and *B. thuringiensis*. (a) Absorption spectra of ThT dissolved in aqueous medium (2 mM Tris buffer, pH 8.5; optical path length = 0.5 cm). The dotted line represents the spectrum of ThT recorded before any treatment [$C_{ThT}^{(0)} = 35 \mu\text{M}$]. The solid line corresponds to a spectrum of the supernatant after the dye solution was incubated with *B. globigii* endospores (8×10^7 spores ml^{-1}) for 10 min and the spores were removed using centrifugation. The decrease in the absorbance corresponds to an $8 \mu\text{M}$ decrease in the ThT concentration: i.e., the concentration of ThT which remained free in the solution after the spore uptake was $28 \pm 2 \mu\text{M}$. (The error bar represents ± 1 standard deviation.) Considering that the volume of a single *B. globigii* spore is about 8×10^{-13} ml, the average ThT concentration in the stained spores was 0.11 M, yielding a distribution coefficient, K_D , of $3.9 \times 10^3 \pm 0.4 \times 10^3$. (b) Contour plot depicting the dependence of the ThT K_D for *B. thuringiensis* endospores on the initial dye concentration, $C_{ThT}^{(0)}$, and on the spore count, SC. The lines represent $K_D[C_{ThT}^{(0)}, SC]$, with the identical values designated by the corresponding numbers tagged to the lines.

certainty. This statistical analysis demonstrated the preferred feasibility for using a power law (equation 3), instead of linear relation, for correlating emission intensity with chromophore concentration.

Binding affinity of ThT for endospores. In addition to the increase in the emission quantum yield of ThT upon binding to the endospores, accumulation of the dye in the endospores will also enhance the imaging contrast of the fluorescently stained species. The distribution coefficient, K_D , for ThT allowed us to quantify the propensity of the dye to accumulate in bacterial endospores:

$$K_D = \frac{C_{\text{spore}}}{C_{\text{solution}}} \tag{4}$$

where C_{spore} and C_{solution} are the concentrations of ThT in the endospore and in the aqueous solution, respectively, after completion of the staining process.

We incubated known amounts of endospores in ThT solutions with preset concentrations and absorbance (Fig. 7a). After the incubation, we centrifuged the endospores and collected the supernatant. From the absorbance of the supernatant, we determined C_{solution} (Fig. 7a). The difference between the absorbance of the ThT prior to the endospore treatment and the absorbance of the supernatant allowed us to estimate the amount of dye that was bound to the endospores and removed from the solution via the centrifugation step. Therefore, $C_{\text{spore}} = n_{ThT} / n_S V_S$, where n_{ThT} is the moles of ThT bound to the endospores, n_S is the number of endospores, and V_S is the volume of a single endospore estimated from their images.

For *B. globigii*, we obtained a K_D of 4×10^3 (Fig. 7a). For *G. stearothermophilus*, a similar approach of incubating 2×10^7 spores ml^{-1} in a $17 \mu\text{M}$ solution of ThT yielded a K_D of 7×10^3 . The measured distribution coefficient, K_D , exhibited dependence on the spore count, SC, and on the initial dye concentration, $C_{ThT}^{(0)}$, in which the spores were incubated. An

increase in $C_{ThT}^{(0)}$ and a decrease in SC caused an increase in K_D (Fig. 6b). This concentration dependence of K_D reflected the fact that a two-state/two-phase model (equation 4) did not encompass the complexity of the dye uptake by the endospores. Nevertheless, the estimated K_D values ranged between about 10^3 and 10^4 , and these values were indicative of the high propensity of ThT to accumulate in bacterial endospores: i.e., the average concentration of ThT in the endospores exceeded by three orders of magnitude the dye concentration in the surrounding aqueous medium. Therefore, the fluorescence staining of endospores with ThT is driven not only by the increase in the emission quantum yield of ThT upon uptake but also by the high propensity of endospores to take up ThT.

Imaging in the presence of contaminants. Despite the established pronounced affinity of ThT for β -amyloid types of protein structures prevalent in endospores and in the cell walls of vegetative bacteria (17, 20, 42, 60–63), binding of the positively charged chromophore (Fig. 1) to a range of other macromolecular structures presents a limitation for employing ThT as a stain for biomedical and environmental samples.

We examined the capability of ThT to selectively stain bacterial endospores in the presence of the following: a biochemical contaminant, DNA; a biomedical contaminant, fetal bovine serum (FBS); and an environmental contaminant, humic acid (HA) (41, 79). The presence of these contaminants, indeed, increased the level of background fluorescence as reflected by the decrease in the DC component of the signal-to-noise ratios (equation 1): S/N_{DC} values were $5.5 \text{ dB} \pm 1.7 \text{ dB}$, $2.5 \text{ dB} \pm 0.2 \text{ dB}$, and $1.8 \text{ dB} \pm 1.5 \text{ dB}$ for the endospore-containing DNA, FBS, and HA samples, respectively (see the supplemental material).

While phase-contrast and differential interference contrast (DIC) microscopies provide the means for visualization of bacterial endospores in relatively pure samples (12, 46, 98), they fail when substantial amounts of particulate contaminants

are present. Fluorescence microscopy of ThT-stained samples, on the other hand, appears to have the potential for visualizing bacterial endospores even when such contaminants are abundantly present.

DISCUSSION

In this study, we hypothesized that an amyloid histology stain, thioflavin T (Fig. 1), allows for visualization of bacterial endospores via fluorescence imaging. To test this hypothesis, we employed a range of optical spectroscopy and microscopy techniques. The experimental evidence not only allows for accepting the hypothesis but also elucidates some of the governing processes leading to the desirable staining outcomes.

What is the relationship among the observations from the three different techniques, of spectroscopy, imaging, and dye distribution analysis? To answer this question, it is essential to consider the heterogeneous nature of the samples. The fluorescence spectra present the intensity of the light emitted from all dye molecules that are in the sample volume illuminated by the excitation beam. Therefore, the spectra encompass the emission from the weakly fluorescent ThT that is free in solution and from the strongly fluorescent ThT that is taken up by the endospores. By far, most of the dye molecules in the stained samples are free in solution (Fig. 7). As previously reported, an increase in the medium viscosity causes an increase in the ThT fluorescence quantum yield (82), which is expected given the properties of chromophores, such as ThT, classified as molecular rotors (4, 81). A viscosity-induced increase in the emission quantum yield of ThT amounts to about three orders of magnitude (82). Therefore, due to the relatively viscous microenvironment of the dye molecules bound within the endospores, the free ThT in the aqueous medium has an emission quantum yield that is about two to three orders of magnitude smaller than the quantum yield of ThT taken up by the spores.

For example, in samples containing 10^6 spores ml^{-1} , the total volume of the spores is about 10^6 times smaller than the volume of the aqueous medium (i.e., the volume of a single spore is on the order of a femtoliter). The measured distribution coefficients, K_D , of about 10^3 to 10^4 , indicate that in such samples only about 0.1% to 1% of the dye is taken up by the endospores. While the number of dye molecules in the aqueous medium is about 100 to 1,000 times more than the number of dye molecules in the endospores, the dye in the aqueous medium has a fluorescence quantum yield about two to three orders of magnitude smaller than that of the endospore-bound dye, which explains the relatively "moderate" emission enhancement (less than an order of magnitude for 10^6 spores ml^{-1}) spectroscopically observed (Fig. 5 and 6). For this discussion, we considered the presence of negligible perturbation in the absorption of ThT when binding to the spores (as evident from the absorption and excitation spectra [Fig. 5a and 6a, respectively]), and we did not include the multiple pathways of excitation and emitted light due to the scattering nature of the samples.

Because an increase in $C_{\text{ThT}}^{(0)}$ (within the micromolar range) tends to decrease K_D (Fig. 7b), the endospore-induced enhancement of the emission of ThT is more pronounced for lower dye concentrations (compare Fig. 5b to Fig. 6b and c).

Thus, diluting the ThT staining solutions tends to improve the extent of the endospore-induced emission enhancement essential for spectroscopic and imaging applications. The sensitivity of the measurements, the background emission from endogenous fluorophores (no matter how weak it might be), the photostability of ThT, and the upper limit of K_D impose limitations on how low $C_{\text{ThT}}^{(0)}$ feasibly can be.

We readily imaged endospores using 1 nM ThT (see the supplemental material), and we demonstrated excellent correlations between spore count and emission intensity for 1 μM ThT (Fig. 6b). These findings demonstrate an immensely wide working range of ThT concentrations, providing the basis for a broad applicability and optimization for each specific application that might resort to ThT-aided spectrofluorometry and imaging.

How do the images relate to the spectroscopic findings? The imaged contrast ratio between the fluorescence intensity corresponding to ThT-stained endospores, $\langle \Delta h \rangle + \Delta I$, and the emission intensity from the free ThT in the background, ΔI (Fig. 3), considerably exceeds one and even two orders of magnitude. The endospores, however, occupy only a few percent (or less) of the total area of the images. As a result, the cumulative intensity from the pixels corresponding to the stained endospores does not exceed by more than about an order of magnitude the cumulative intensity from the pixels corresponding to the image background. This trend is in agreement with the fluorescence enhancement observed from the spectral data.

Overall, the accumulation of ThT in the bacterial endospores increases the local dye concentration, followed by an increase in the amount of light absorbed and emitted by the stained endospores. The increase in the ThT emission quantum yield upon endospore uptake further enhances the intensity of the emitted light from the stained regions. The synergy between these two effects is essential for attaining images with sufficiently large signal-to-noise ratios, essential for visualization of bacterial endospores with acceptable contrast, especially when the background autofluorescence signal is prevalent.

Where does ThT bind? This study does not provide a direct answer. Indeed, ThT targets β -amyloid-type proteins with high affinity (43), and bacterial endospores are coated with β -strand proteins as evident, for example, from high-resolution atomic force microscopy (AFM) images (60–63). These facts provide the rationale of this study for staining endospores with ThT, which targets their endogenous protein structures. The images of the ThT-stained endospores showed bright contours outlining their elliptical shapes, which is consistent with the dye collecting in the surface regions of the spores (where the high β -protein content has been demonstrated [60–63]), and with an increase in the fluorescence quantum yield of the dye bound to these endospore surface regions. Our evidence does not rule out the possibility for weakly fluorescent ThT present in the interior of the stained endospores. The pronounced density of intact endospores, however, suppresses facile diffusion of molecular species with the size of ThT into their interior (contributing to the resilience of these dormant species). Furthermore, unless endogenous fluorescence quenchers are present, the rigid interior of endospores entrapping the dye and re-

straining its molecular motions will cause an increase in its fluorescence quantum yield (82). Therefore, most probably, the emission intensity of the ThT-stained endospore images represents the dye distribution throughout these dormant bacterial entities.

Furthermore, ThT staining did not noticeably affect the viability of bacterial endospores. Cell culture tests of endospores incubated in various concentrations of ThT revealed that staining with this dye does not compromise the ability of endospores to germinate (see supplemental material). Thus, ThT either does not bind to key components of the endospores essential for their germination or does not negatively affect these molecular components even if it binds to them.

What are the practical implications of the endospore-induced ThT fluorescence enhancement? The tight correlations between the emission enhancement and the spore count (Fig. 5b and 6b) illustrate the applicability of the use of ThT for spectroscopic quantification of endospore suspensions. Such spectroscopic measurements, however, are immensely susceptible to the presence of contaminants, such as vegetative bacterial cells, environmental polymers, and blood proteins. Such restrictions, therefore, limit the ThT spectrofluorometry to pure endospore samples.

For imaging, on the other hand, ThT presents unexplored potentials. Based on their morphology, ThT-stained bacterial endospores are readily discernible in the presence of vegetative bacterial cells (Fig. 4). Debris of lysed cells (due to sporulation, for example) does not compromise the visualization of the endospores (Fig. 4d). Furthermore, staining with ThT provides means for facile visualization of bacterial endospores in the presence of macromolecular contaminants that not only enhance the ThT fluorescence but also contribute to the autofluorescence of the sample (see the supplemental material).

Speed and ease are the principal advantages of using amyloid stains for imaging bacterial endospores. The mild ambient conditions under which the administration of such stains is conducted along with the absence of any pre- and/or posttreatment steps provide important and unique capabilities for this approach of fluorescence imaging. Therefore, while classical methods for staining endospores, such as the Schaeffer-Fulton stain, require a series of thermal fixing and wash steps, mixing of the ThT solution with the bacterial sample without any further treatment allowed for simultaneous staining of vegetative bacteria and endospores during sporulation (Fig. 2d). ThT amyloid stain provides an unprecedented facility for fluorescence imaging of bacterial endospores.

Conclusions. The ability of ThT to stain bacterial endospores was driven by its binding affinity and by the increase in its fluorescence quantum yield upon uptake. While a variety of stains for vegetative cells are available for bioanalytical assays and imaging with minimal treatment, the choice of methodologies for enhancement and visualization of bacterial endospores is somewhat limited. Our demonstration of fluorescence imaging with an amyloid histology stain exhibits venues for utilization of alternative endogenous markers (such as β -folded protein aggregates) for facile and expedient bioanalytical applications targeting bacterial endospores, known for their resilience and structural stability.

ACKNOWLEDGMENTS

Funding for this research was provided by the U.S. Army Research Laboratory (to G.J.), by the National Science Foundation (grant CBET 0935995 to V.I.V.), by the UC Regents' Faculty Development Award (to V.I.V.), and by the National Institutes of Health (grant 2R01-DC02775-06 to B.A.).

We extend our gratitude to B. Hyle Park for the discussions on image analysis.

REFERENCES

1. Ankolekar, C., T. Rahmati, and R. G. Labbe. 2009. Detection of toxigenic *Bacillus cereus* and *Bacillus thuringiensis* spores in U.S. rice. *Int. J. Food Microbiol.* **128**:460–466.
2. Arnon, S. S., et al. 2001. Botulinum toxin as a biological weapon: medical and public health management. *JAMA* **285**:1059–1070.
3. Bao, D., et al. 2009. Electrochemical oxidation of ferrocene: a strong dependence on the concentration of the supporting electrolyte for nonpolar solvents. *J. Phys. Chem. A* **113**:1259–1267.
4. Bao, D., et al. 2010. Electrochemical reduction of quinones: interfacing experiment and theory for defining effective radii of redox moieties. *J. Phys. Chem. B* **114**:14467–14479.
5. Belgrader, P., et al. 1999. PCR detection of bacteria in seven minutes. *Science* **284**:449–450.
6. Beverly, M. B., K. J. Voorhees, T. L. Hadfield, and R. B. Cody. 2000. Electron monochromator mass spectrometry for the analysis of whole bacteria and bacterial spores. *Anal. Chem.* **72**:2428–2432.
7. Biancalana, M., and S. Koide. 2010. Molecular mechanism of thioflavin-T binding to amyloid fibrils. *Biochim. Biophys. Acta* **1804**:1405–1412.
8. Bisset, K. A. 1950. Evolution in bacteria and the significance of the bacterial spore. *Nature* **166**:431–432.
9. Cable, M. L., et al. 2009. Detection of bacterial spores with lanthanide-macrocyclic binary complexes. *J. Am. Chem. Soc.* **131**:9562–9570.
10. Cable, M. L., J. P. Kirby, K. Sorasaenec, H. B. Gray, and A. Ponce. 2007. Bacterial spore detection by [Tb³⁺(macrocyclic)(dipicolinate)] luminescence. *J. Am. Chem. Soc.* **129**:1474–1475.
11. Chau, K., et al. 2011. Dependence of the quality of adhesion between poly(dimethylsiloxane) and glass surfaces on the composition of the oxidizing plasma. *Microfluid. Nanofluid.* **10**:907–917.
12. Chen, D., S. S. Huang, and Y. Q. Li. 2006. Real-time detection of kinetic germination and heterogeneity of single bacillus spores by laser tweezers Raman spectroscopy. *Anal. Chem.* **78**:6936–6941.
13. Dobson, C. M. 2003. Protein folding and misfolding. *Nature* **426**:884–890.
14. Driks, A. 2003. The dynamic spore. *Proc. Natl. Acad. Sci. U. S. A.* **100**:3007–3009.
15. Eaton, D. F. 1990. Recommended methods for fluorescence decay analysis. *Pure Appl. Chem.* **62**:1631–1648.
16. Fichtel, J., J. Koester, J. Rullkoetter, and H. Sass. 2007. Spore dipicolinic acid contents used for estimating the number of endospores in sediments. *FEMS Microbiol. Ecol.* **61**:522–532.
17. Fowler, D. M., A. V. Koulov, W. E. Balch, and J. W. Kelly. 2007. Functional amyloid—from bacteria to humans. *Trends Biochem. Sci.* **32**:217–224.
18. Franz, D. R., et al. 1997. Clinical recognition and management of patients exposed to biological warfare agents. *JAMA* **278**:399–411.
19. Fyke, E. M., B. Langseth, J. S. Olsen, G. Skogan, and J. M. Blatny. 2008. Detection of bioterror agents in air samples using real-time PCR. *J. Appl. Microbiol.* **105**:351–358.
20. Gebbink, M. F., D. Claessen, B. Bouma, L. Dijkhuizen, and H. A. Wösten. 2005. Amyloids—a functional coat for microorganisms. *Nat. Rev. Microbiol.* **3**:333–341.
21. Groenning, M., et al. 2007. Binding mode of thioflavin T in insulin amyloid fibrils. *J. Struct. Biol.* **159**:483–497.
22. Gueltekin, A., A. Ersoez, N. Y. Sarioezlue, A. Denizli, and R. Say. 2010. Nanosensors having dipicolinic acid imprinted nanoshell for *Bacillus cereus* spores detection. *J. Nanopart. Res.* **12**:2069–2079.
23. Hammer, N. D., X. Wang, B. A. McGuffie, and M. R. Chapman. 2008. Amyloids: friend or foe? *J. Alzheimer's Dis.* **13**:407–419.
24. Harel, M., L. K. Sonoda, I. Silman, J. L. Sussman, and T. L. Rosenberry. 2008. Crystal structure of thioflavin T bound to the peripheral site of torpedo californica acetylcholinesterase reveals how thioflavin T acts as a sensitive fluorescent reporter of ligand binding to the acylation site. *J. Am. Chem. Soc.* **130**:7856–7861.
25. Hindle, A. A., and E. A. Hall. 1999. Dipicolinic acid (DPA) assay revisited and appraised for spore detection. *Analyst* **124**:1599–1604.
26. Hisamatsu, H., and K. Maekawa. 1994. The distribution of the Durbin-Watson statistic in integrated and near-integrated models. *J. Econom.* **61**:367–382.
27. Hong, C., D. Bao, M. S. Thomas, J. M. Clift, and V. I. Vullev. 2008. Print-and-peel fabrication of microelectrodes. *Langmuir* **24**:8439–8442.
28. Hu, J., et al. 2009. Long-lived photogenerated states of alpha-oligothio-

- phene-acridinium dyads have triplet character. *J. Phys. Chem. A* **113**:3096–3107.
29. Inglesby, T. V., et al. 2002. Anthrax as a biological weapon, 2002: updated recommendations for management. *JAMA* **287**:2236–2252.
 30. Iqbal, S. S., et al. 2000. A review of molecular recognition technologies for detection of biological threat agents. *Biosens. Bioelectron.* **15**:549–578.
 31. Jakob-Roetne, R., and H. Jacobsen. 2009. Alzheimer's disease: from pathology to therapeutic approaches. *Angew. Chem. Int. Ed. Eng.* **48**:3030–3059.
 32. Jones, G., II, et al. 1995. Photoinduced electron transfer for pyrenesulfonamide conjugates of tryptophan-containing peptides. Mitigation of fluorophore behavior in N-terminal labeling experiments. *Bioorg. Med. Chem. Lett.* **5**:2385–2390.
 33. Jones, G., II, V. Vullev, E. H. Braswell, and D. Zhu. 2000. Multistep photoinduced electron transfer in a *de novo* helix bundle: multimer self-assembly of peptide chains including a chromophore special pair. *J. Am. Chem. Soc.* **122**:388–389.
 34. Jones, G., II, and V. I. Vullev. 2001. Contribution of a pyrene fluorescence probe to the aggregation propensity of polypeptides. *Org. Lett.* **3**:2457–2460.
 35. Jones, G., II, and V. I. Vullev. 2001. Ground- and excited-state aggregation properties of a pyrene derivative in aqueous media. *J. Phys. Chem. A* **105**:6402–6406.
 36. Jones, G., II, and V. I. Vullev. 2002. Medium effects on the photophysical properties of terbium(III) complexes with pyridine-2,6-dicarboxylate. *Photochem. Photobiol. Sci.* **1**:925–933.
 37. Jones, G., II, and V. I. Vullev. 2002. Medium effects on the stability of terbium(III) complexes with pyridine-2,6-dicarboxylate. *J. Phys. Chem. A* **106**:8213–8222.
 38. Jones, G., II, and V. I. Vullev. 2002. Photoinduced electron transfer between non-native donor-acceptor moieties incorporated in synthetic polypeptide aggregates. *Org. Lett.* **4**:4001–4004.
 39. Jones, G., II, et al. 2007. Photoinduced electron transfer in arylacridinium conjugates in a solid glass matrix. *J. Phys. Chem. B* **111**:6921–6929.
 40. Jones, G., II, X. Zhou, and V. I. Vullev. 2003. Photoinduced electron transfer in alpha-helical polypeptides: dependence on conformation and electron donor-acceptor distance. *Photochem. Photobiol. Sci.* **2**:1080–1087.
 41. Jones, G., II, and G. L. Indig. 1996. Spectroscopic and chemical binding properties of humic acids in water. *New J. Chem.* **20**:221–232.
 42. Jordal, P. B., et al. 2009. Widespread abundance of functional bacterial amyloid in mycolata and other Gram-positive bacteria. *Appl. Environ. Microbiol.* **75**:4101–4110.
 43. Khurana, R., et al. 2005. Mechanism of thioflavin T binding to amyloid fibrils. *J. Struct. Biol.* **151**:229–238.
 44. Kim, K., et al. 2005. Rapid genotypic detection of *Bacillus anthracis* and the *Bacillus cereus* group by multiplex real-time PCR melting curve analysis. *FEMS Immunol. Med. Microbiol.* **43**:301–310.
 45. Klunk, W. E., et al. 2001. Uncharged thioflavin-T derivatives bind to amyloid-beta protein with high affinity and readily enter the brain. *Life Sci.* **69**:1471–1484.
 46. Kong, L. B., P. F. Zhang, P. Setlow, and Y. Q. Li. 2010. Characterization of bacterial spore germination using integrated phase contrast microscopy, Raman spectroscopy, and optical tweezers. *Anal. Chem.* **82**:3840–3847.
 47. Kricka, L. J., and P. Fortina. 2009. Analytical ancestry: "firsts" in fluorescent labeling of nucleosides, nucleotides, and nucleic acids. *Clin. Chem.* **55**:670–683.
 48. Kukreja, R. V., S. K. Sharma, and B. R. Singh. 2010. Molecular basis of activation of endopeptidase activity of botulinum neurotoxin type E. *Biochemistry* **49**:2510–2519.
 49. LeVine, H., III. 1993. Thioflavine T interaction with synthetic Alzheimer's disease beta-amyloid peptides: detection of amyloid aggregation in solution. *Protein Sci.* **2**:404–410.
 50. Ljosa, V., and A. E. Carpenter. 2008. High-throughput screens for fluorescent dye discovery. *Trends Biotechnol.* **26**:527–530.
 51. Maji, S. K., et al. 2009. Functional amyloids as natural storage of peptide hormones in pituitary secretory granules. *Science* **325**:328–332.
 52. Makino, S., and H. Cheun. 2003. Application of the real-time PCR for the detection of airborne microbial pathogens in reference to the anthrax spores. *J. Microbiol. Methods* **53**:141–147.
 53. Maskevich, A. A., et al. 2007. Spectral properties of thioflavin T in solvents with different dielectric properties and in a fibril-incorporated form. *J. Proteome Res.* **6**:1392–1401.
 54. Millare, B., et al. 2008. Dependence of the quality of adhesion between polydimethyl siloxane and glass surfaces on the conditions of treatment with oxygen plasma. *Langmuir* **24**:13218–13224.
 55. Montecucco, C., and J. Molgó. 2005. Botulinum neurotoxins: revival of an old killer. *Curr. Opin. Pharmacol.* **5**:274–279.
 56. Naiki, H., K. Higuchi, M. Hosokawa, and T. Takeda. 1989. Fluorometric determination of amyloid fibrils invitro using the fluorescent dye, thioflavine-T. *Anal. Biochem.* **177**:244–249.
 57. Nicholson, W. L., N. Munakata, G. Horneck, H. J. Melosh, and P. Setlow. 2000. Resistance of bacillus endospores to extreme terrestrial and extraterrestrial environments. *Microbiol. Mol. Biol. Rev.* **64**:548–572.
 58. Ohhashi, Y., M. Kihara, H. Naiki, and Y. Goto. 2005. Ultrasonication-induced amyloid fibril formation of beta(2)-microglobulin. *J. Biol. Chem.* **280**:32843–32848.
 59. Pellegrino, P. M., N. F. Fell, Jr., D. L. Rosen, and J. B. Gillespie. 1998. Bacterial endospore detection using terbium dipicolinate photoluminescence in the presence of chemical and biological materials. *Anal. Chem.* **70**:1755–1760.
 60. Plomp, M., T. J. Leighton, K. E. Wheeler, H. D. Hill, and A. J. Malkin. 2007. In vitro high-resolution structural dynamics of single germinating bacterial spores. *Proc. Natl. Acad. Sci. U. S. A.* **104**:9644–9649.
 61. Plomp, M., T. J. Leighton, K. E. Wheeler, and A. J. Malkin. 2005. Architecture and high-resolution structure of *Bacillus thuringiensis* and *Bacillus cereus* spore coat surfaces. *Langmuir* **21**:7892–7898.
 62. Plomp, M., T. J. Leighton, K. E. Wheeler, M. E. Pitesky, and A. J. Malkin. 2005. *Bacillus atrophaeus* outer spore coat assembly and ultrastructure. *Langmuir* **21**:10710–10716.
 63. Plomp, M., and A. J. Malkin. 2009. Mapping of proteomic composition on the surfaces of bacillus spores by atomic force microscopy-based immunolabeling. *Langmuir* **25**:403–409.
 64. Premasiri, W. R., et al. 2005. Characterization of the surface enhanced Raman scattering (SERS) of bacteria. *J. Phys. Chem. B* **109**:312–320.
 65. Rao, S. S., K. V. Mohan, and C. D. Atreya. 2010. Detection technologies for *Bacillus anthracis*: prospects and challenges. *J. Microbiol. Methods* **82**:1–10.
 66. Rosen, D. L. 1999. Bacterial endospore detection using photoluminescence from terbium dipicolinate. *Rev. Anal. Chem.* **18**:1–21.
 67. Rosen, D. L., C. Sharpless, and L. B. McGown. 1997. Bacterial spore detection and determination by use of terbium dipicolinate photoluminescence. *Anal. Chem.* **69**:1082–1085.
 68. Rueckert, A., R. S. Ronimus, and H. W. Morgan. 2005. Development of a rapid detection and enumeration method for thermophilic bacilli in milk powders. *J. Microbiol. Methods* **60**:155–167.
 69. Rutledge, D. N., and A. S. Barros. 2002. Durbin-Watson statistic as a morphological estimator of information content. *Anal. Chim. Acta* **454**:277–295.
 70. Sadik, O. A., W. H. Land, and J. Wang. 2003. Targeting chemical and biological warfare agents at the molecular level. *Electroanalysis* **15**:1149–1159.
 71. Schaeffer, A., and M. D. Fulton. 1933. A simplified method of staining endospores. *Science* **77**:194.
 72. Singh, P. K., M. Kumbhakar, H. Pal, and S. Nath. 2010. Ultrafast bond twisting dynamics in amyloid fibril sensor. *J. Phys. Chem. B* **114**:2541–2546.
 73. Singh, P. K., M. Kumbhakar, H. Pal, and S. Nath. 2009. Ultrafast torsional dynamics of protein binding dye thioflavin-T in nanoconfined water pool. *J. Phys. Chem. B* **113**:8532–8538.
 74. Singh, P. K., M. Kumbhakar, H. Pal, and S. Nath. 2010. Viscosity effect on the ultrafast bond twisting dynamics in an amyloid fibril sensor: thioflavin-T. *J. Phys. Chem. B* **114**:5920–5927.
 75. Slieman, T. A., and W. L. Nicholson. 2001. Role of dipicolinic acid in survival of *Bacillus subtilis* spores exposed to artificial and solar UV radiation. *Appl. Environ. Microbiol.* **67**:1274–1279.
 76. Snyder, A. P., A. Tripathi, J. P. Dworzanski, W. M. Maswadeh, and C. H. Wick. 2005. Characterization of microorganisms by thermogravimetric analysis-mass spectrometry. *Anal. Chim. Acta* **536**:283–293.
 77. Song, J. M., M. Culha, P. A. Kasili, G. D. Griffin, and T. Vo-Dinh. 2005. A compact CMOS biochip immunosensor towards the detection of a single bacteria. *Biosens. Bioelectron.* **20**:2203–2209.
 78. Steele, P. T., et al. 2005. Desorption/ionization fluence thresholds and improved mass spectral consistency measured using a flattop laser profile in the bioaerosol mass spectrometry of single bacillus endospores. *Anal. Chem.* **77**:7448–7454.
 79. Steinberg, C. E., T. Meinelt, M. A. Timofeyev, M. Bittner, and R. Menzel. 2008. Humic substances. *Environ. Sci. Pollut. Res. Int.* **15**:128–135.
 80. Stratis-Cullum, D. N., G. D. Griffin, J. Mobley, A. A. Vass, and T. Vo-Dinh. 2003. A miniature biochip system for detection of aerosolized *Bacillus globigii* spores. *Anal. Chem.* **75**:275–280.
 81. Stsiapura, V. I., et al. 2008. Thioflavin T as a molecular rotor: fluorescent properties of thioflavin T in solvents with different viscosity. *J. Phys. Chem. B* **112**:15893–15902.
 82. Sulatskaya, A. I., A. A. Maskevich, I. M. Kuznetsova, V. N. Uversky, and K. K. Turoverov. 2010. Fluorescence quantum yield of thioflavin T in rigid isotropic solution and incorporated into the amyloid fibrils. *PLoS One* **5**:e15385.
 83. Taylor, K. M. L., and W. Lin. 2009. Hybrid silica nanoparticles for luminescent spore detection. *J. Mater. Chem.* **19**:6418–6422.
 84. Thomas, M. S., J. M. Clift, B. Millare, and V. I. Vullev. 2010. Print-and-peel fabricated passive micromixers. *Langmuir* **26**:2951–2957.
 85. Thomas, M. S., et al. 2010. Print-and-peel fabrication for microfluidics: what's in it for biomedical applications? *Ann. Biomed. Eng.* **38**:21–32.
 86. Thomas, M. S., et al. 2010. Kinetics of bacterial fluorescence staining with 3,3'-diethylthiacyanine. *Langmuir* **26**:9756–9765.
 87. Uithoven, K. A., J. C. Schmidt, and M. E. Ballman. 2000. Rapid identification of biological warfare agents using an instrument employing a light addressable potentiometric sensor and a flow-through immunofiltration-enzyme assay system. *Biosens. Bioelectron.* **14**:761–770.

88. **Vasquez, J. M., A. Vu, J. S. Schultz, and V. I. Vullev.** 2009. Fluorescence enhancement of warfarin induced by interaction with beta-cyclodextrin. *Bio-technol. Prog.* **25**:906–914.
89. **Vetri, V., et al.** 2007. Amyloid fibrils formation and amorphous aggregation in concanavalin A. *Biophys. Chem.* **125**:184–190.
90. **Voropai, E. S., et al.** 2003. Spectral properties of thioflavin T and its complexes with amyloid fibrils. *J. Appl. Spectrosc.* **70**:868–874.
91. **Vullev, V. I., and G. Jones.** 2002. Photoinduced electron transfer in alkanoylpyrene aggregates in conjugated polypeptides. *Tetrahedron Lett.* **43**: 8611–8615.
92. **Vullev, V. I., et al.** 2006. Nonlithographic fabrication of microfluidic devices. *J. Am. Chem. Soc.* **128**:16062–16072.
93. **Wan, J., et al.** 2008. Solvent dependence of the charge-transfer properties of a quaterthiophene-anthraquinone dyad. *J. Photochem. Photobiol. A Chem.* **197**:364–374.
94. **Wan, J., M. S. Thomas, S. Guthrie, and V. I. Vullev.** 2009. Surface-bound proteins with preserved functionality. *Ann. Biomed. Eng.* **37**:1190–1205.
95. **Wictome, M., et al.** 1999. Development of an *in vitro* bioassay for *Clostridium botulinum* type B neurotoxin in foods that is more sensitive than the mouse bioassay. *Appl. Environ. Microbiol.* **65**:3787–3792.
96. **Xing, Y., and K. Higuchi.** 2002. Amyloid fibril proteins. *Mech. Ageing Dev.* **123**:1625–1636.
97. **Yang, W.-W., and A. Ponce.** 2009. Rapid endospore viability assay of *Clostridium sporogenes* spores. *Int. J. Food Microbiol.* **133**:213–216.
98. **Zhang, P. F., L. B. Kong, G. W. Wang, P. Setlow, and Y. Q. Li.** 2010. Combination of Raman tweezers and quantitative differential interference contrast microscopy for measurement of dynamics and heterogeneity during the germination of individual bacterial spores. *J. Biomed. Opt.* **15**:056010.
99. **Zhang, X. Y., M. A. Young, O. Lyandres, and R. P. Van Duyne.** 2005. Rapid detection of an anthrax biomarker by surface-enhanced Raman spectroscopy. *J. Am. Chem. Soc.* **127**:4484–4489.

Amyloid Histology Stain for Rapid Bacterial Endospore Imaging (Supplemental Material)

Bing Xia,¹ Srigokul Upadhyayula,^{2,3} Vicente Nuñez,² Pavel Landsman,¹
Samuel Lam,³ Harbani Malik,² Sharad Gupta,² Mohammad Sarshar,² Jingqiu Hu,¹
Bahman Anvari,² Guilford Jones,¹ and Valentine I. Vullev^{2,3,4,*}

Department of Chemistry and Photonics Center, Boston University, Boston, MA 02215.¹ Department of Bioengineering and Center for Bioengineering Research, University of California, Riverside, CA 92521.² Department of Biochemistry, University of California, Riverside, CA 92521.³ Department of Chemistry, University of California, Riverside, CA 92521.⁴

SUPPLEMENTAL MATERIALS AND METHODS

Materials. For the imaging studies, thioflavin T (>95 % purity, Aldrich, Milwaukee, WI) was used as received. For some of the spectroscopy studies, the dye was further purified via recrystallization as a hexafluorophosphate salt. Comparison of the UV/visible absorption and emission spectra of the purified and the commercial-purity dye, however, did not reveal any detectable differences.

All other reagents, spectroscopic grade, were purchased from VWR and from Fisher Scientific. The buffered aqueous solutions were prepared using Millipore H₂O and filtered through 0.2 µm polycarbonate syringe filters (Corning) before use. The notion of lowered protein binding affinity of ThT in acidic media (3), along with improved protein-induced fluorescence enhancement in slightly alkaline media (1), governed our choice of buffering the samples for this study at pH between 8.5 and 9. The absorption and excitation spectra showed that under the employed conditions, the used weakly alkaline media does not induce hydroxylation of ThT, as previously reported for elevated temperatures and prolonged exposure to aqueous media (2).

For contaminant studies, the deoxyribonucleic acid (DNA) was extracted from and purified using QIAGEN Plasmid Maxi Kit (purchased from QIAGEN Inc., Valencia, CA), humic acid and fetal bovine serum were purchased from Fischer Scientific.

Bacterial samples. Bacterial endospore cultures: (i) *B. subtilis*, *B. globigii* and *Bacillus thuringiensis* (*B. thuringiensis*) were obtained from U.S. Army Research Laboratory facility, as desiccated powders. (ii) *B. atropheaus* and *G. stearothermophilus* were purchased from SPS Medical (Rush, NY) in the form of 20% ethanol aqueous suspension. They were stored at 2°C suspended in deionized double distilled water (DDW) or in 40 % ethanol – DDW.

Before assays, all suspended cultures were washed with ice-cold DDW at least 5 times. They were then kept at 2°C or on ice until use. Lyophilized endospores were resuspended and repeatedly washed with ice-cold deionized double distilled water. Prior to measurements, endospores or particles were transferred to the corresponding buffered dye-free solution, resuspended, sonicated 2-3 times (15 sec. per pulse) and kept on ice. After mixing with the dye stock solutions (in the same buffer or in water), the samples were sonicated 1-2 times. In

several comparative experiments, Tween® 20 or Tween® 40 (7) (0.1 % w/v) or alcohol (20 – 40 % v/v) was used to facilitate handling (resuspension washing and centrifugation) of several endospore samples; no essential difference was observed in the thioflavin T reactivity of the samples thus treated, as compared with the control.

Endospores were counted under a phase contrast microscope (Nikon, magnification × 400), using a Petroff-Hausser chamber (VWR). Concentrated endospore stocks were diluted toward final count $5 \times 10^8 - 3 \times 10^9$ per ml and stored up to one week at 2°C in the dark until use. Standard count error was 10 – 20 %. Phase-contrast microscopic appearance of the water-washed endospore samples before purification confirmed them as essentially pure (90 – 97 % endospores). Large (about 4 - 10 µm) endospore aggregates and other organic particles of uncertain origin (apparently resembling large particulates reported in previously examined endospore specimens (8)) occurred in the lyophilized endospore samples in minor quantities. No vegetative cells were observed in endospore cultures studied.

Vegetative bacteria cultures: *Escherichia coli* (*E. coli*), TOP 10 cells, were obtained from Invitrogen (Carlsbad, CA); and wild type *B. subtilis* were obtained from ATCC (Manassas, VA). Primary *Bacillus* cultures (18 hrs) of vegetative bacteria were outgrown from endospores in 2 % LB medium (Sigma) at 30°C. The cultures were then washed with plenty of cold DDW. They appeared under microscope as viable colonies of average size 2-10 cells, characteristic of *Bacillus*. These bacteria were then treated, counted, and directly assayed. For sporulation, the *Bacillus* vegetative cells were plated and grown on thin layers of LB Agar for 10 days at 37 °C, and the growth was swabbed to collect the formed endospores.(5)

Contaminant samples. Large quantities of plasmid DNA were extracted from *E. coli* cells strain DH5a (transformed with NSP1 gene; Clone Id: YJL041W) using a standard QIAGEN maxi prep kit, and methods described in the Quick-Start protocol handbook. The used buffer volumes were adjusted based on the size of the cell pellet. Concentration of the purified plasmid DNA was obtained spectroscopically via pre-calibrated standard curve. Plasmid DNA was used as a contaminant at a final concentration of 1 mg ml⁻¹, and was spiked with spores (or no spores added for controls).

Humic acid contaminant samples were prepared at a final concentration of 1 mg ml⁻¹, without additional processing, and were spiked with spores if needed. Stock fetal bovine serum was diluted (1:1 v/v) with 2 mM Tris buffer, pH 8.5, and was spiked or not spiked with spores. The controls (samples without spores) and half of the spore-containing samples were stained with ThT for 5 minutes and imaged.

Optical imaging. Bright field and fluorescence images of bacterial samples were acquired using a Nikon Ti-U inverted microscope (Nikon Inc., Melville, NY), equipped with a 100× Nikon oil immersion objective (N.A. = 1.49, WD = 120 mm). A 100-watt Xenon arc lamp (LUDL Electronic products, Hawthorne, NY), in combination with a FITC filter set ($l_{\text{ex}} = 482$, $l_{\text{em}} = 536$ nm, band widths = 25 nm, Chroma Technology, Bellows Falls, VT), was used for fluorescence imaging. The images were recorded with a Hamamatsu EM-CCD digital camera (model C9100-13, Hamamatsu Corp., Bridgewater, NJ) controlled by HImage application software; and saved in a 16-bit gray-scale format: i.e., $2^{16} = 65,536$ hues of gray for each pixel, where 0 corresponds to black (no signal) and 65,535 corresponds to white (maximum light intensity / saturation). Image analysis of the gray-scale distribution was performed using Igor Pro software v.6.02A (Wavemetrics) installed on Windows and Mac OS workstations as we have previously demonstrated.

Signal-to-noise ratios of images. The signal-to-noise ratios, S/N , were calculated from the horizontal or vertical gray-scale traces across each of the imaged spores (Figure S1). While S/N is defined as a decimal logarithm of the ratio between the power of the signal and the power of the noise (that for the same image can be estimated from the square of the ratio between the amplitude of the signal and the amplitude of the noise), in the fluorescence microscope images the noise has direct current, DC, and alternative current, AC, components. The amplitude of the DC noise, A_{DC} , is extracted from the dark background of the image (Figure S1b); and the amplitude of the AC noise, A_{AC} , is estimated

from the root-mean-square of the fluctuations of the background (Figure S1c):

$$A_{AC} = RMS = \sqrt{\frac{1}{n} \sum_{i=1}^n (I_i - A_{DC})^2} \quad (S1a)$$

$$A_{DC} = \frac{1}{n} \sum_{i=1}^n I_i \quad (S1b)$$

where n is the number of “background” pixels analyzed and I_i is the intensity of pixel i .

The AC and DC contributions to S/N were estimated separately (eq. 1 and S1) using the noise amplitudes and the average heights, $\langle h \rangle$, of the peaks on the traces crossing over imaged spores (Figure S1b, c).

For each set of imaging conditions, we obtained the S/N values as an average of the gray-scale trace analysis (Figure S1) of at least ten imaged spores from multiple images, located in different quadrants of the images.

Spectroscopy. Absorption spectra were recorded using DU-640B Beckman spectrophotometer and JASCO V-670 UV/Vis/NIR spectrophotometer. Steady-state emission spectra were recorded using Felix/Timemaster spectrofluorometer (Photon Technology International, Inc.), using slit width 10 nm; and Fluorolog-3-22 spectrofluorometer (Horiba Jobin Yvon) using slit widths between 2 and 5 nm. All measurements were performed at ambient temperature, in polystyrene 2-sided and 4-sided cuvettes, with 1 cm optical paths (unless stated otherwise), after 10 – 15 min. pre-incubation in dark. Calibration and purity confirmation measurements of thioflavin T were reproduced in quartz cuvettes. The thioflavin T concentrations for all samples were estimated from its apparent molar absorption coefficient at peak wavelength 412 nm ($36,000 \pm 500 \text{ M}^{-1} \text{ cm}^{-1}$) (3).

Microplate reader fluorescence measurements with thioflavin T were performed in triplicates in black 96-well plates (Greiner), using SpectraMax Gemini XS fluorescence plate reader (Molecular Devices), at excitation wavelengths

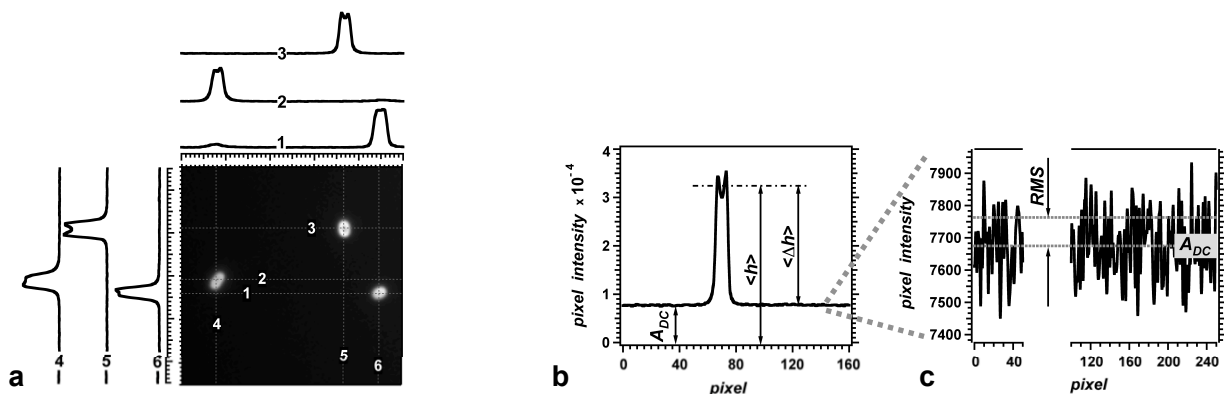


Figure S1. Signal-to-noise analysis of an epifluorescence microscopy image of *B. atrophaeus* endospores suspended in a 100 μM solution of ThT (2 mM Tris buffer, pH 8.5). (a) Microscopy image with corresponding horizontal and vertical traces crossing through the fluorescent spores (exposure time = 4 s). (b) Designation of trace parameters: $A_{DC} = 7.7 \times 10^3$; $\langle h \rangle = 3.2 \times 10^4$; $\langle \Delta h \rangle = 2.4 \times 10^4$. (c) The trace baseline with average value of A_{DC} and $RMS = 90$. The data for the trace on (b) and (c) yield $S/N_{AC} = 69$ dB, and $S/N_{DC} = 12$ dB (eq. 1 and S1).

430 nm and emission wavelength 495 nm, with filter cutoff 475 nm, after 2 min. shaking and 15 min. pre-incubation in dark. The pH of the aqueous solutions was monitored using an Orion 420A pH meter. Data analysis and calculations were performed using Igor Pro software v.6.02A (Wavemetrics) installed on Windows and Mac OS workstations.

Dye distribution. The distribution coefficients, K_D , are defined as the concentration ratios between the dye taken up by the spores and the dye remained in solution (eq. 3). The values of C_{SPORE} and $C_{SOLUTION}$ were extracted from spectroscopic data.

The samples were prepared by incubating a 1 ml solution of varying concentrations of thioflavin T (ThT) with known count of bacterial endospores for 10 minutes under constant stirring. (The 10-minute period ensured completion of the staining processes, which we determined using kinetic measurements as we previously demonstrated.) The ThT-endospore mixture was centrifuged for two minutes at 12,000 rpm, using Eppendorf Centrifuge 5415 with a rotational radius of 7.5 cm, and the supernatant was collected. (The spectra were averaged from at least three different experiments for the same species and spore counts.) Using the molar extinction coefficient values, ThT concentrations were estimated from the absorption spectra. For these studies, we selected dye concentrations and cuvette thicknesses that yielded absorbance values in the range between 0.10 and 1.0. For $A < 0.1$, less than 20 % of the light is absorbed by the sample; and for $A > 1$, the sample absorbs more than 90% of the light permitting analysis based on changes only within less than 10% of the incident light intensity.

Approximating the shape of the endospores to an ellipsoid (i.e., prolate spheroid), allowed us to estimate the volume of a single endospore, $V_s = (4/3)\pi a^2 b$, where a and b are the short and long elliptic radii, respectively, estimated from the images of the endospores. The decrease in the absorbance at 412 nm, after the incubation and centrifugation steps, provided information about the amount (moles) of dye taken up by the endospores. Dividing the amount of taken up dye by the endospore volume, yielded the average ThT concentration in the endospores, C_{SPORE} (eq. 3). $C_{SOLUTION}$ needed for calculating the distribution coefficient (eq. 3) was obtained from the absorption of the supernatant.

SUPPLEMENTAL RESULTS

Staining of bacterial endospores with ThT. The dynamic range of the recording equipment placed limits on the S/N improvement resultant from extending the exposure time. Indeed, an increase in the exposure time increased not only the signal, but also the noise. For spore samples treated with 100 μM ThT, exposure time of 5 to 7 s allowed for attaining the maximum signal intensity, i.e., $\langle h \rangle \approx 6 \times 10^4$ (Figure 2d). Extending the exposure time beyond 7 s, thus, did not increase the signal (i.e., led to saturation), but increased the noise, i.e., A_{AC} and RMS (Figure S2a). As a corollary, extended exposure

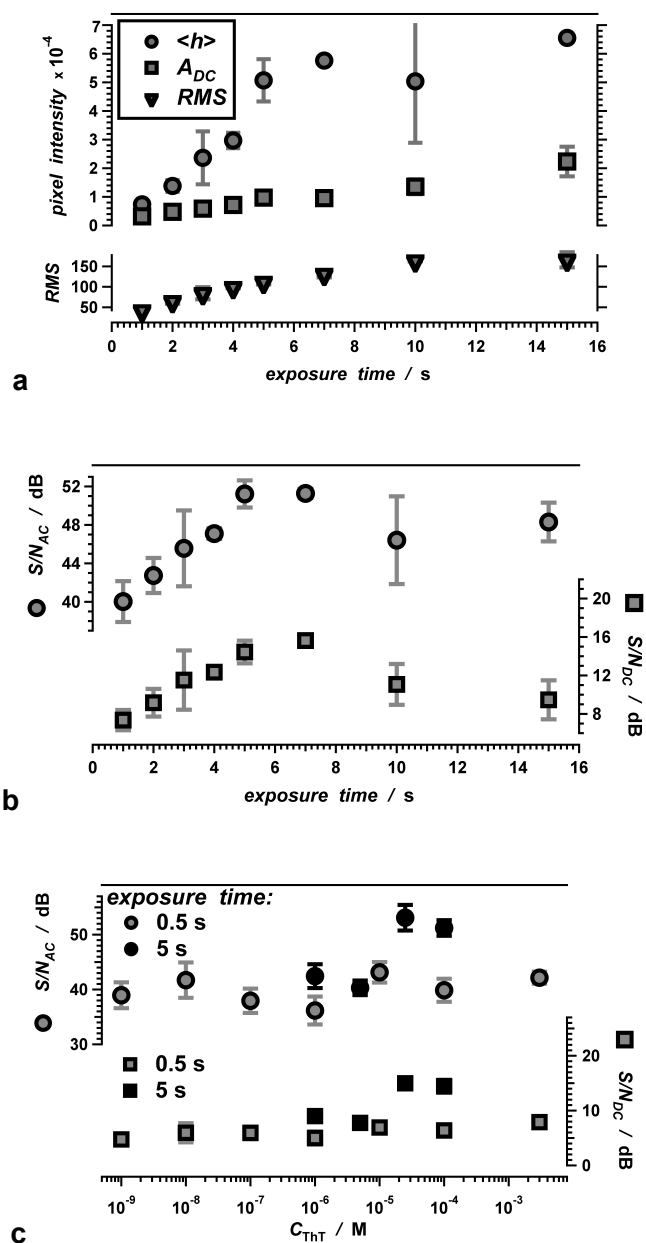


Figure S2. Dependence of signal-to-noise ratios, S/N , on exposure time and on dye concentration, C_{ThT} , for epifluorescence images of *B. atrophaeus* endospores suspended in ThT solution (2 mM Tris buffer, pH 8.5). (a) Dependence of the amplitude of the signal, $\langle h \rangle$, and the amplitudes of the DC and AC noise, A_{DC} and RMS , respectively, on the exposure time for $C_{ThT} = 100 \mu\text{M}$. (b) Dependence of the AC and DC noise on the exposure time for $C_{ThT} = 100 \mu\text{M}$. (c) Dependence of the AC and DC noise on the ThT concentration for exposure time = 0.5 s and 5 s.

times (beyond ~ 7 s) resulted in deterioration of the measured S/N (Figure S2b).

The ThT concentration, C_{ThT} , had a less pronounced effect on the S/N , especially for short exposure times (Figure S2c). For 0.5-s exposure time, varying C_{ThT} over six orders of magnitude affected neither S/N_{AC} , nor S/N_{DC} (Figure S2c). For relatively short exposure times (e.g., 1 s), the baseline RMS

manifested no dependence on C_{ThT} ; and the background fluorescence from the free ThT, ΔI , contributed less than $\sim 15\%$ to the intensity of A_{DC} (Figure 2c, e). Conversely, for exposure times extending to 5 s, the optimal S/N_{AC} and S/N_{DC} appeared optimal for C_{ThT} in the range of tens and hundred μM (Figure S2c).

In aqueous media, ThT aggregates as its concentration increases above about $1\ \mu\text{M}$ (4, 6). An improved staining ability of aggregated ThT (4), therefore, can be an underlying plausible reason for the observed improvement in the image S/N as C_{ThT} is raised above $10^{-6}\ \text{M}$.

It should be emphasized that it is S/N_{AC} that presents limitation for improving the quality of images. For processing of small signals on large DC background, inherent for numerous spectroscopic and imaging techniques, analogue or

digital subtraction of A_{DC} from the whole data set immensely improves S/N_{DC} , and the overall S/N . Improving S/N_{AC} , however, is considerably more challenging and less straightforward than the relatively facile optimization of S/N_{DC} . The images of the fluorescently stained endospores manifested $A_{DC} \gg RMS$, and hence $S/N_{AC} > S/N_{DC}$, revealing the promising potentials of ThT for facile visualization of dormant bacterial cells.

Cell-culture tests of endospores incubated in various concentrations of ThT revealed that staining with this dye does not compromise their ability to germinate (Figure S3).

Imaging in the presence of contaminants. Despite the relatively low S/N_{DC} values, the stained spores were still visualizable in the presence of the contaminants (Figure S4e, j, o). Although the presence of the contaminants also compromised the AC component of S/N (eq. 1b), the S/N_{AC} values were still large enough to allow for visualization of the endospores. The signals from the stained endospores noticeably surpassed the background baseline noise, and S/N_{AC} was $40\ \text{dB} \pm 4\ \text{dB}$, $35\ \text{dB} \pm 1\ \text{dB}$ and $28\ \text{dB} \pm 10\ \text{dB}$ for the endospore containing DNS, FBA and HA samples, respectively.

The presence of DNA had no detectable effect on S/N_{AC} and a mildly noticeable effect on S/N_{DC} . Among the three contaminants, however, HA proved to be the most challenging for the ThT staining and the fluorescence imaging of the endospores. Nevertheless, S/N_{AC} exceeding 10 dB (even for the HA samples) still provide means for achieving acceptable image contrasts for visualizing the endospores.

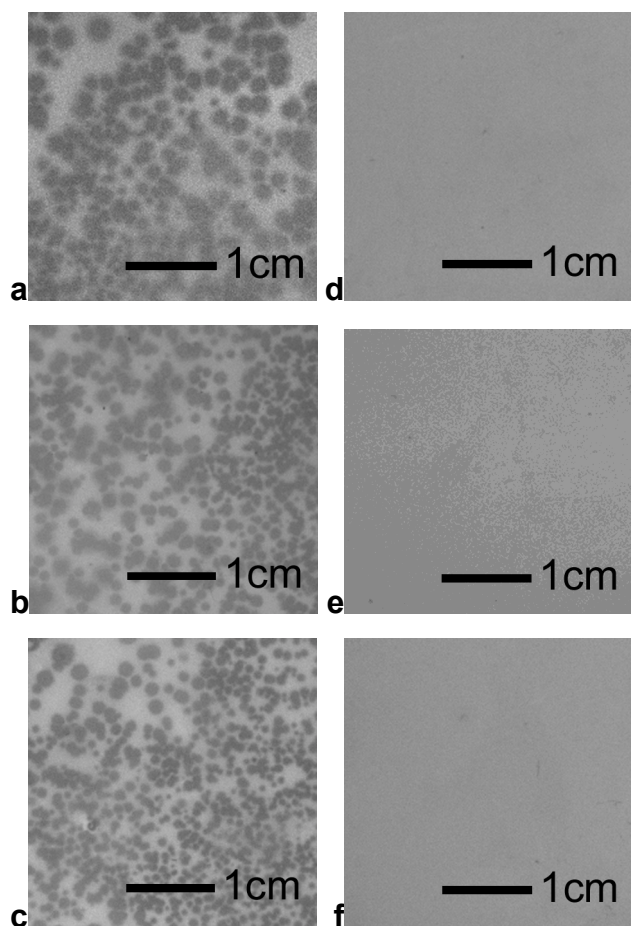


Figure S3. Solid cultures of *B. atrophaeus* plated from endospore suspensions (10^6 spore ml^{-1} , 2 mM Tris buffer, pH 8.5) in 7.5-cm Petri dishes. The endospores were suspended in a solution of (a) 0 μM , (b) 100 μM and (c) 3 mM ThT for > 10 min prior to plating. Similar plating with endospore-free buffer solutions containing: (d) no ThT (e) 100 μM and (f) 3 mM, did not produce detectable colonies.

SUPPLEMENTAL REFERENCES

1. Eisert, R., L. Felau, and L. R. Brown. 2006. Methods for enhancing the accuracy and reproducibility of Congo red and thioflavin T assays. *Analytical Biochemistry* **353**:144-146.
2. Fodera, V., M. Groenning, V. Vetri, F. Librizzi, S. Spagnolo, C. Cornett, L. Olsen, M. van de Weert, and M. Leone. 2008. Thioflavin T hydroxylation at basic pH and its effect on amyloid fibril detection. *Journal of Physical Chemistry B* **112**:15174-15181.
3. Groenning, M., M. Norrman, J. M. Flink, M. van de Weert, J. T. Bukrinsky, G. Schluckebier, and S. Frokjaer. 2007. Binding mode of thioflavin T in insulin amyloid fibrils. *Journal of Structural Biology* **159**:483-497.
4. Khurana, R., C. Coleman, C. Ionescu-Zanetti, S. A. Carter, V. Krishna, R. K. Grover, R. Roy, and S. Singh. 2005. Mechanism of thioflavin T binding to amyloid fibrils. *Journal of Structural Biology* **151**:229-238.
5. Powers, E. M. 1968. Method for obtaining free bacterial spores of *Bacillus subtilis* var. Niger. *Applied Microbiology* **16**:180-181.
6. Schirra, R. 1985. Dye aggregation in freezing aqueous-solutions. *Chemical Physics Letters* **119**:463-466.
7. Turnbough, C. L. 2003. Discovery of phage display peptide ligands for species-specific detection of bacillus spores. *Journal of Microbiological Methods* **53**:263-271.
8. Williams, D. D., and C. L. Turnbough, Jr. 2004. Surface layer protein eal is not a component of *Bacillus anthracis* spores but is a persistent contaminant in spore preparations. *Journal of Bacteriology* **186**:566-569.

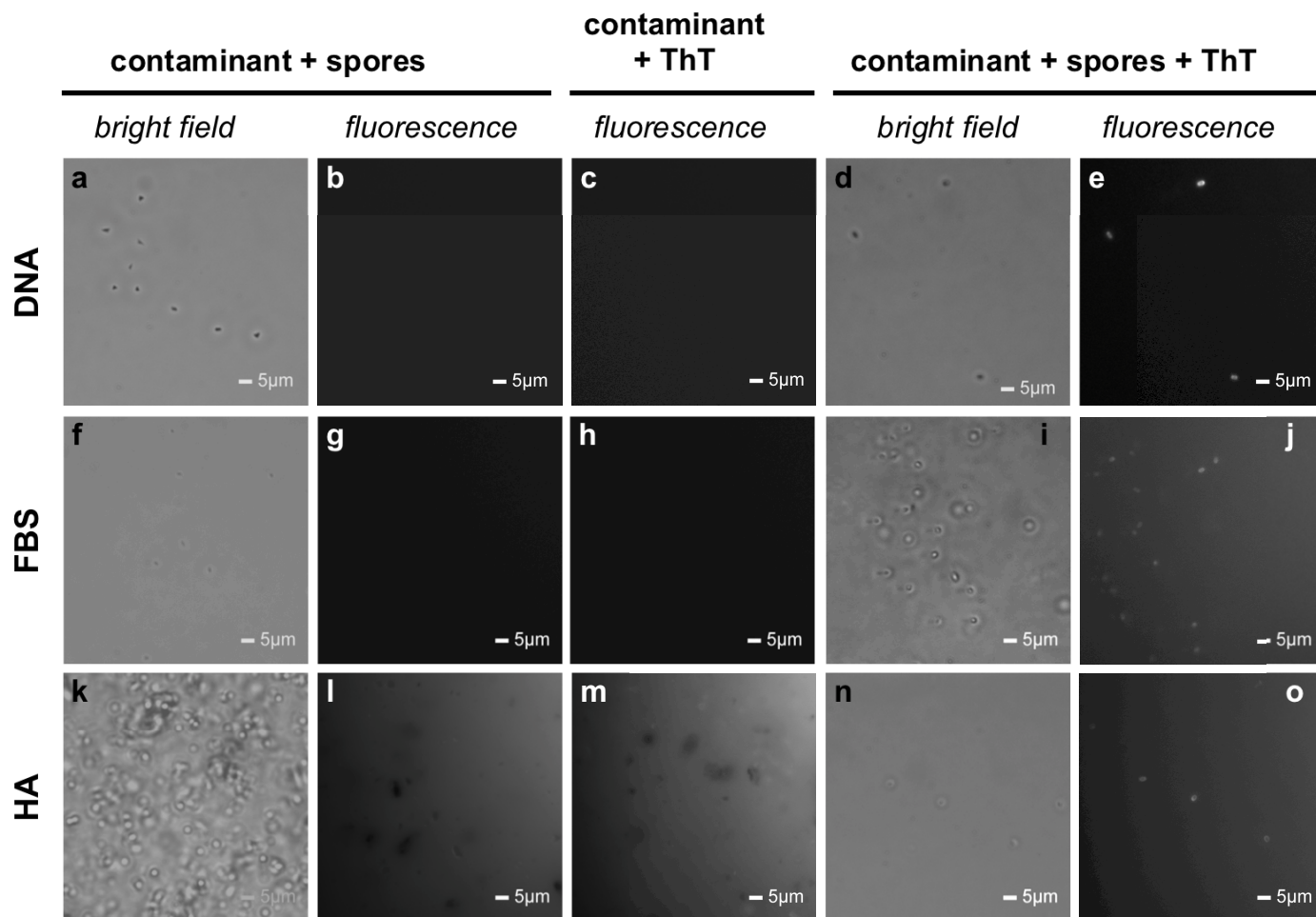


Figure S4. Images of endospores of *B. atrophaeus* suspended in solutions of biological and environmental contaminants: **(a-e)** 1 mg ml^{-1} DNA extract from *E. coli*; **(f-j)** 50% v/v fetal bovine serum (FBS); and **(k-o)** 1 mg ml^{-1} humic acid (HA); dissolved in aqueous buffer (2 mM Tris buffer, pH 8.5; *exposure time* = 0.5 s). The ThT concentration for the stained samples **(c-e, h-j, and m-o)** was $150 \text{ } \mu\text{M}$. The heterogeneity and the pronounced fluorescence of HA (overlapping with the ThT fluorescence range) presented challenges for imaging of the added endospores. We do not have a proof if any of the structures depicted on the bright-field images **(k)** belong to the suspended spores. Staining the sample with ThT, however, allowed for visualization of the spores **(o)** and focusing the objective on them, provided means for observing them even in a bright-field mode **(n)**. Such fluorescence structures were not present in the HA samples without endospores **(m)**.